Electronic Supplementary Material (ESI) for Chemical Communications

Visible-light Driven Plasmonic Photocatalyst Ag/AgCl @ Helical Chiral TiO_2 Nanofibers

Dawei Wang, Yi Li, Gianluca Li Puma, Chao Wang, Peifang Wang, Wenlong Zhang, and Qing Wang*

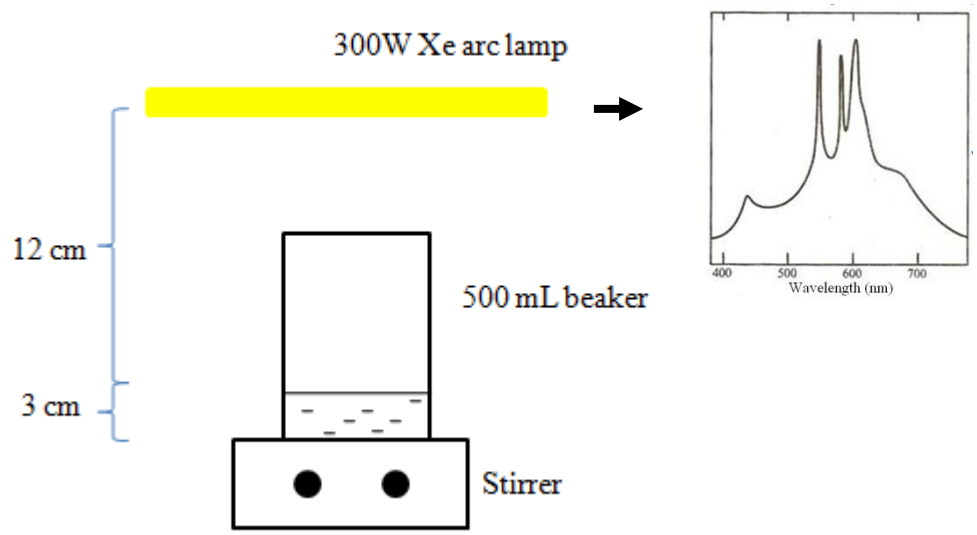

Fig. S1. The reactor of the photocatalytic degradation experiments, the inset picture is the emission spectrum of 300W Xe arc lamp (Philips) with a UV cut-off 25 filter (providing visible light $\lambda \geq 400$ nm).

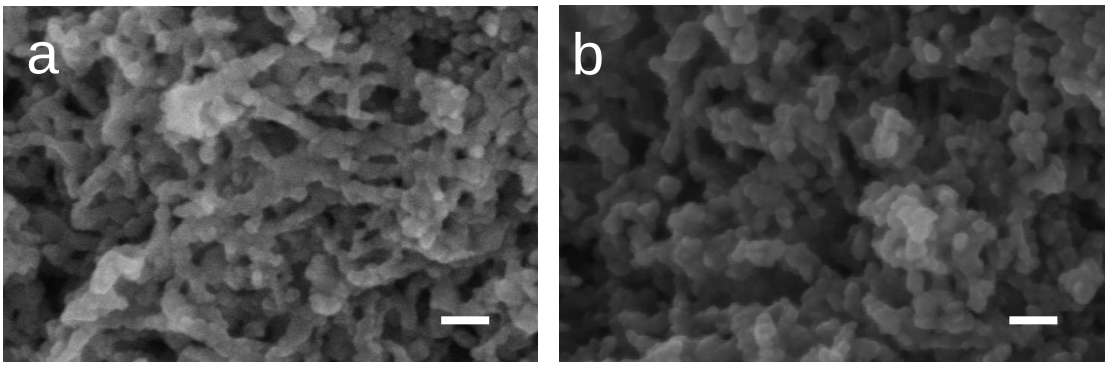

Fig. S2. SEM images of broken chiral TiO_2 nanofibers. **(a)** 4MPa. **(b)** 6MPa. Scale bars in **a** and **b** represent 50 nm both. Some unbroken chiral nanofibers were observed in **a**, some nanofibers were broken after increasing the pressure (**b**), which shows chiral structures were damaged more seriously as the pressure increased.

XRD results

X-ray diffraction (XRD) was used to determine the phase structure of samples. The chiral TiO_2 nanofibers (Fig. S3a) and Ag/AgCl @ broken chiral TiO_2 nanofibers (10MPa) (Fig. S3b) were synthesized as reference compound. The XRD results of Ag/AgCl @ chiral TiO_2 nanofibers (Fig. S3c) showed that metal Ag coexisted with AgCl crystals. The peaks corresponding to Ag and AgCl were also found in Ag/AgCl @ broken chiral TiO_2 nanofibers(10MPa) (Fig.S3b). Other peaks were corresponding to the different TiO_2 crystal phases (JCPDS file) and no peaks of other impurities were detected, indicating that only Ag and AgCl were deposited during the synthesis process.

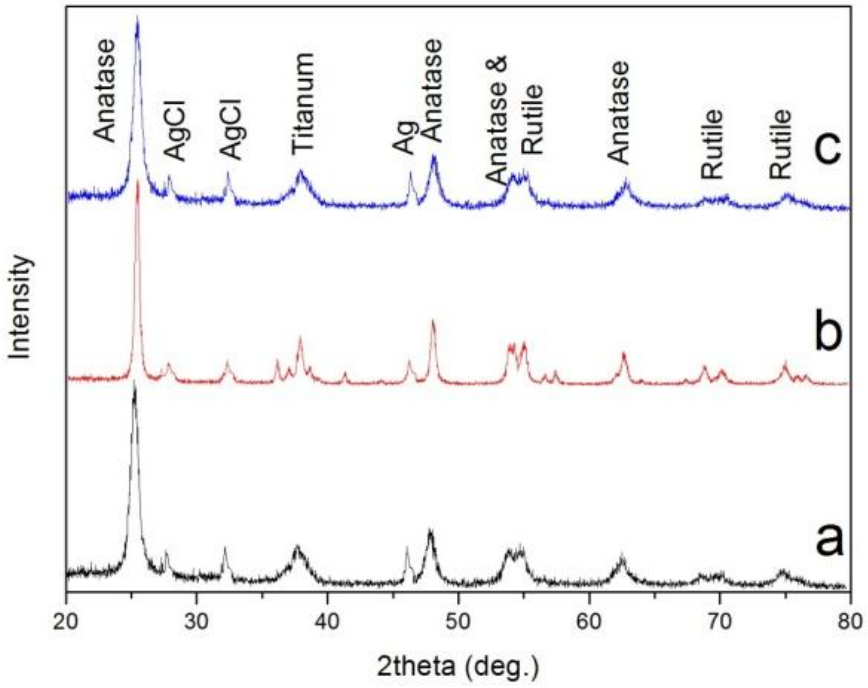

Fig. S3. XRD patterns of (**a**) pure chiral TiO_2 nanofibers, (**b**) Ag/AgCl @ broken chiral nanofibers (10MPa) and (**c**) Ag/AgCl @ chiral TiO_2 nanofibers.

XPS results

The elemental and chemical compositions of the samples were further analyzed by X-ray photoelectron spectroscopy (XPS). The results (Fig. S4) suggest that both Ag/AgCl @ broken chiral TiO_2 nanofibers (10MPa) and Ag/AgCl @ chiral TiO_2 nanofibers contain Ti, O, C, Ag and Cl elements. The C1s is attributed to the adventitious hydrocarbon from the XPS instrument itself[S1]. In Fig. S5, the Ag 3d spectra consists of two individual peaks approximately at 373 and 367 eV, which are due to Ag $3d_{3/2}$ and Ag $3d_{5/2}$ binding energy, respectively. The existence of Ag^0 and Ag^{+1} could be verified by further peaks divisions[S2]. Consequently, the XPS results determined that the nanoparticles deposited on both broken chiral TiO_2 nanofibers and chiral TiO_2 nanofibers were made of Ag/AgCl composites. The EDX elemental atomic composition of Ag (5.49 mol %) and Cl (2.86 mol %) (Fig. S6) indicated that the Ag/AgCl was almost at a 1:1 molar ratio.

Reference

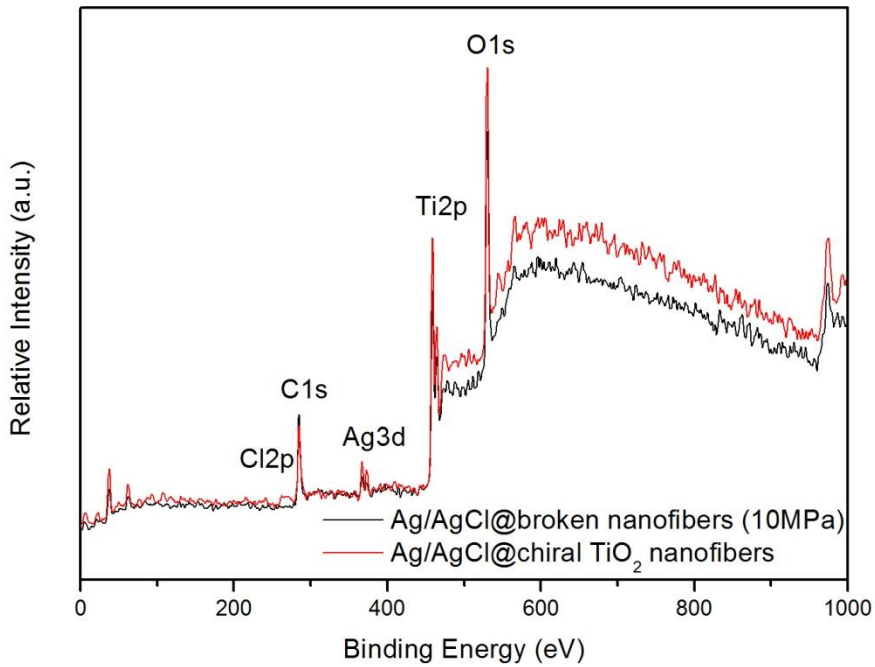

Fig. S4. XPS spectra of all elements of Ag/AgCl @ P25 and Ag/AgCl @ chiral TiO_2 nanofibers.

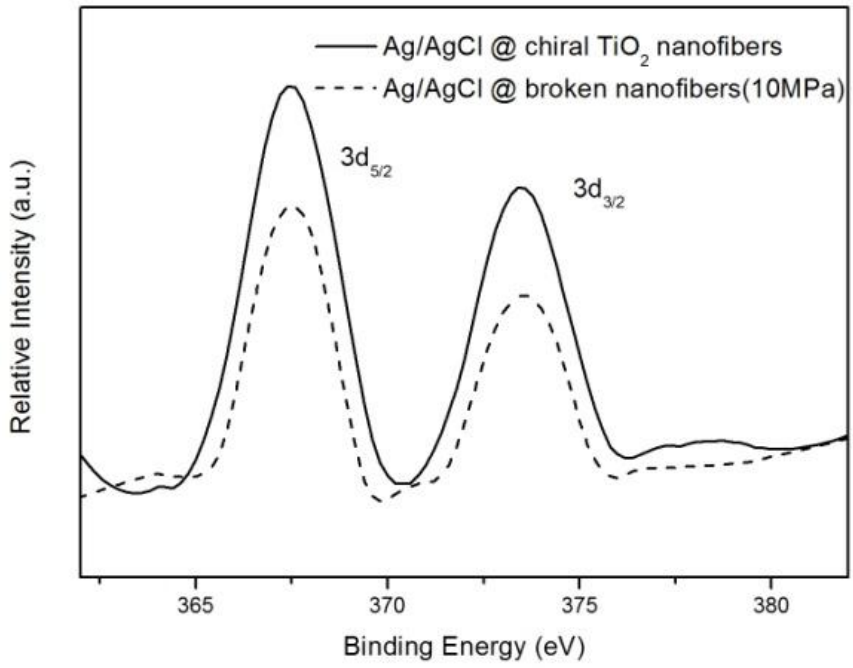

Fig. S5. High-resolution XPS spectra of Ag 3d of Ag/AgCl @ chiral TiO_2 nanofibers and Ag/AgCl @ broken chiral nanofibers (10MPa).

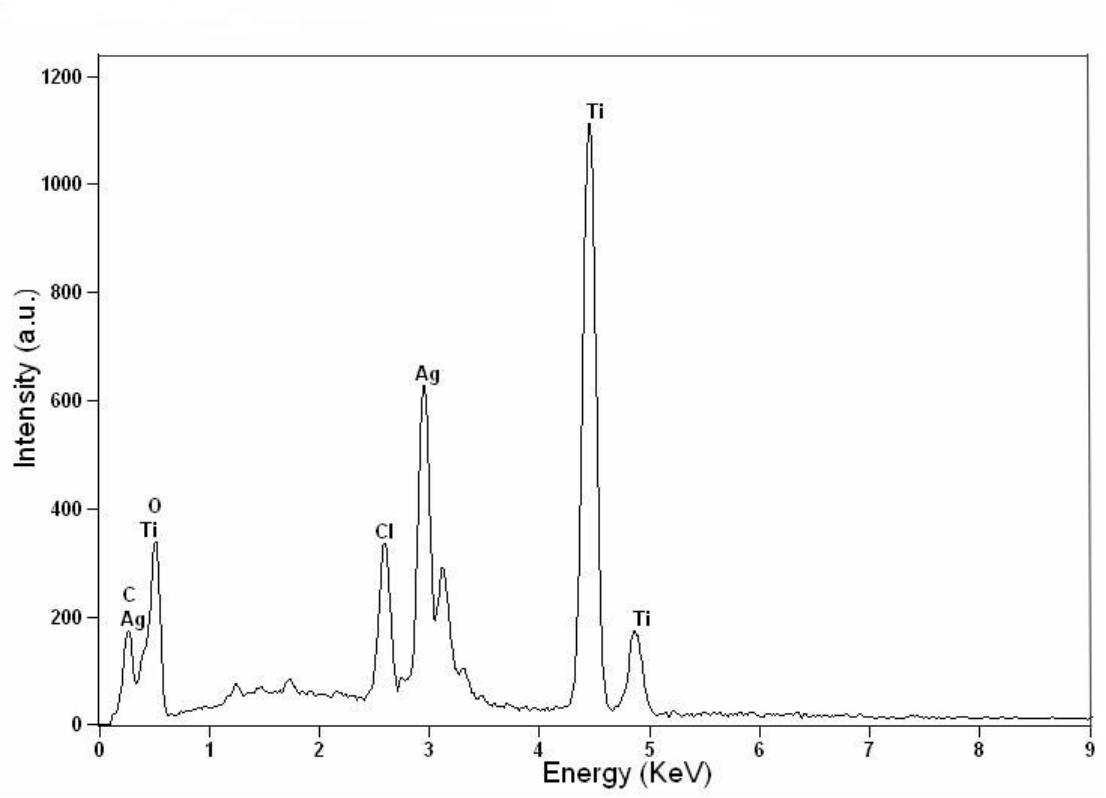

Fig. S6. Corresponding EDX pattern of Ag/AgCl @ chiral TiO_2 nanofibers.

UV-vis results

The UV-visible diffuse reflectance (Fig. S7) of the Ag/AgCl @ chiral TiO_2 nanofibers showed strong absorption in both the ultraviolet and the visible-light regions. The stronger absorption of Ag/AgCl @ chiral TiO_2 nanofibers at 200-350 nm compared to pure chiral TiO_2 nanofibers can be attributed to the characteristic absorption of the AgCl semiconductor[S1], besides, Ag NPs can absorb photons from an area much larger than their geometric cross section. Resonance energy transfer (RET, the transfer of energy from a plasmon to a nearby semiconductor) enhances the electric field intensity thereby increasing the optical absorption[S3]. In contrast, the increased response in the visible-light region (400-800 nm) results from the creation of SPR[S4]. The significant red shift of the absorption edge observed in the Ag/AgCl @ chiral TiO_2 nanofibers (trace c) when compared with Ag/AgCl @ broken chiral TiO_2 nanofibers (trace b), demonstrates that controlled chirality at the nanoscale level induces a greater SPR effect. The nanostructured ordered helical arrangement of the Ag/AgCl nanoparticles induces coupled plasmon waves propagating along the helical path, causing increased absorption of the incident light components that are in tune with the handedness of the helices. The collective plasmons that oscillate along the plasmonic chiral structure of certain handedness lead to different absorptions in response to right- and left- circularly polarized light[S4]. Therefore, the acceleration of SPR excitation results from the nanostructure of ordered Ag/AgCl nanoparticles, which are irradiated at specific incident polarization angles.

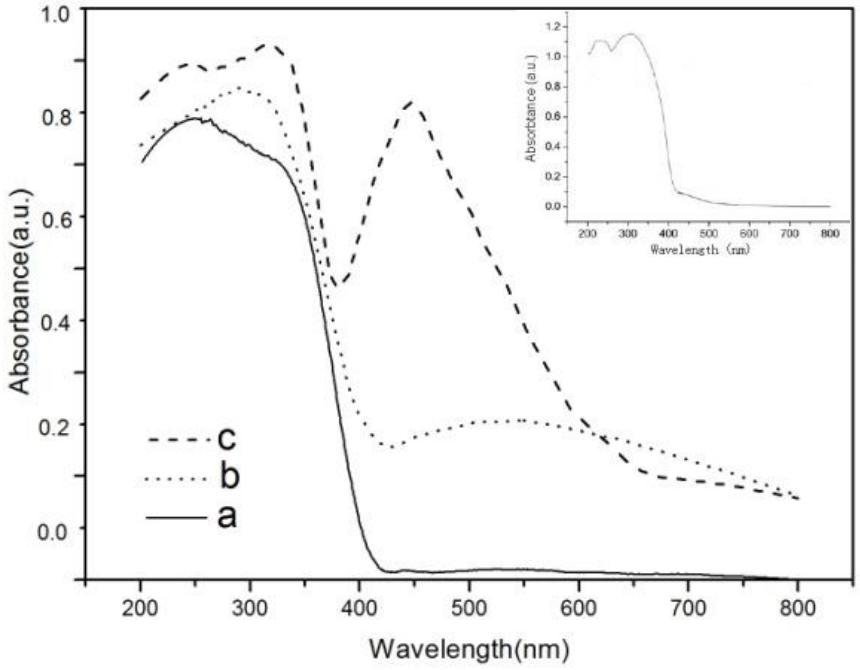

Fig. S7. UV-vis diffuse reflectance spectra of (**a**) pure chiral TiO_2 nanofibers, (**b**) Ag/AgCl @ broken chiral nanofibers (10MPa). (**c**) Ag/AgCl @ chiral TiO_2 nanofibers. The inset shows the UV-vis absorbtion spectrum of AgCl (ref. 10).

Optical thickness

$$\tau = \varepsilon C_{\text{cat}} L \qquad \text{S1}$$

$$\varepsilon = \frac{\int_{\lambda_{\min}}^{\lambda_{\max}} \varepsilon_\lambda I_\lambda \mathrm{d}\lambda}{\int_{\lambda_{\min}}^{\lambda_{\max}} I_\lambda \mathrm{d}\lambda} \qquad \text{S2}$$

Where τ is the optical thickness, ε is average extinction coefficient, C_{cat} is the concentration of catalyst, L is depth of liquid in the reactor traversed by photon beams, λ is the incident light wavelength, I is the incident light intensity,

ε_λ is the specific extinction coefficient which could be calculated by applying Beer-Lambert Law in Fig. S5, λ_{min} and λ_{max} are the minimum and maximum wavelengths of incident light.

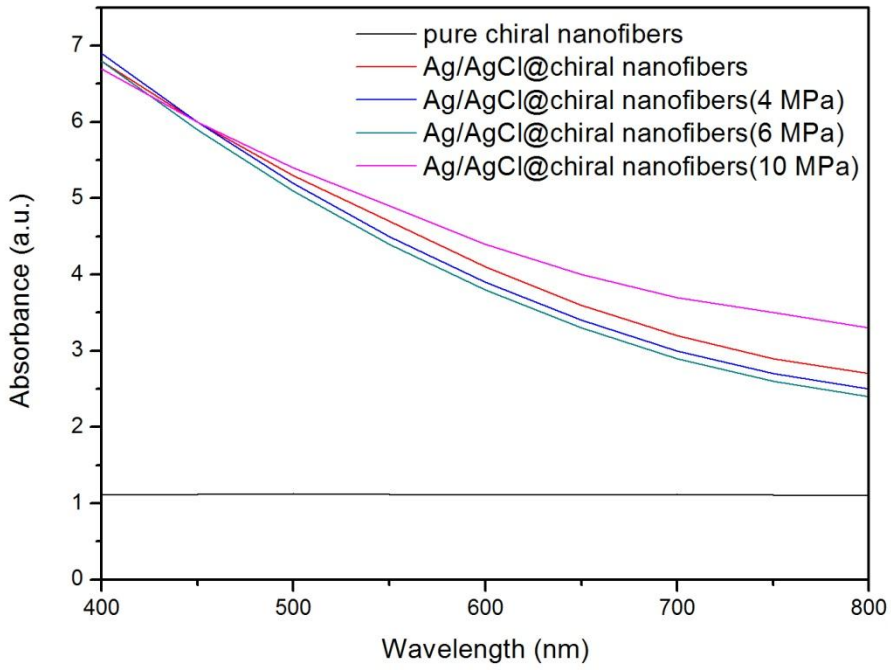

Fig. S8. UV-vis absorption spectroscopy of catalyst suspensions, these were performed when the concentrations of catalyst were 1 g/L (same as the catalyst concentrations in the photocatalytic experiments).

Table. S1. The optical thicknesses of various photocatalysts

Catalyst	Pure chiral nanofibers	Ag/AgCl@ chiral nanofibers	Ag/AgCl@ chiral nanofibers (4 MPa)	Ag/AgCl@ chiral nanofibers (6 MPa)	Ag/AgCl@ chiral nanofibers (10 MPa)
τ	4.15	13.2	12.9	12.7	14.3

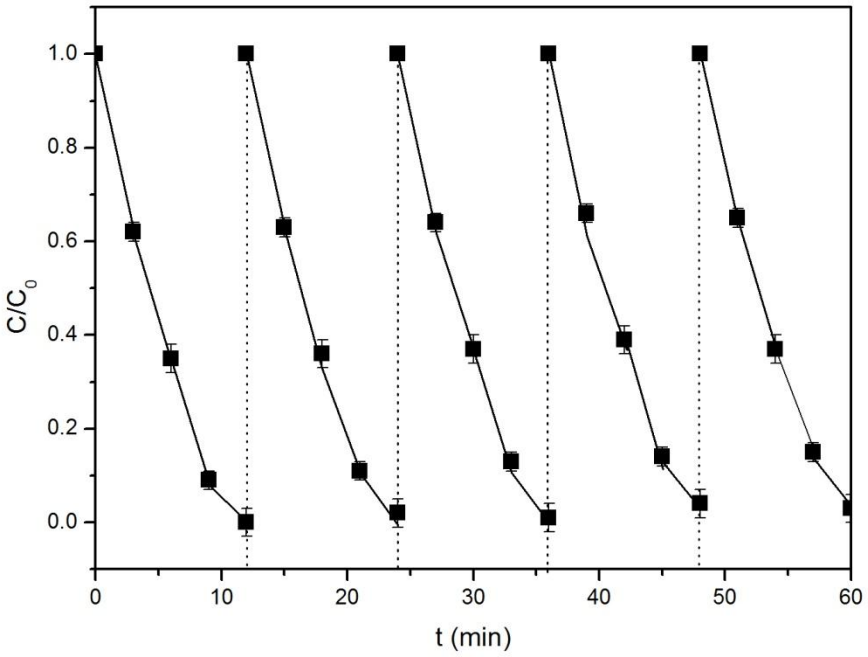

Fig. S9. Cycle photocatalytic degradation of Ag/AgCl @ chiral TiO2 nanofibers

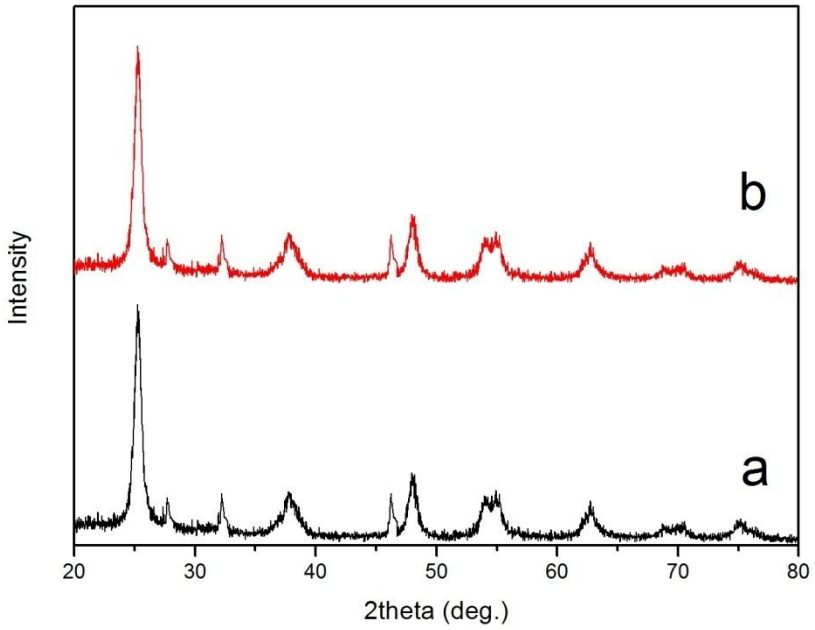

Fig. S10. Comparison of XRD patterns. (**a**) As prepared Ag/AgCl @ chiral TiO_2 nanofibers. (**b**) Ag/AgCl @ chiral TiO_2 nanofibers cycling for 5 times.

Experiments

Preparation: The preparation of chiral TiO_2 nanofibers is similar to the method described by Liu et al. C_{18}-D-Glu was chosen as template for the synthesis of chiral TiO_2 nanofibers (more details see ref. 22). Then, the as-prepared pure chiral TiO_2 nanofibers were used to fabricate Ag/AgCl @ chiral TiO_2 nanofibers. In a typical synthesis of Ag/AgCl @ chiral TiO_2 nanofibers, pure chiral TiO_2 nanofibers (0.2 g) and cetyltrimethyammonium chloride (0.3 g, purchased from TCI) were added into deionized water (100 mL) while stirring at room temperature. After the mixture was stirred for 60 min, $AgNO_3$ (2.0 mL, 0.1 M) was quickly added into the mixture. The resulting solution was stirred at room temperature for further 60 min and irradiated with a 8W UV light for 40 min. The suspension was collected by centrifugal separation and then dried at 80 °C for 8 h, which resulted in a brown powder. Finally, the powder was calcined at 300 °C. Chiral TiO_2 nanofibers were also physically broken with the application of pressure at 4, 6 and 10 MPa using FTIR tablet press (to avoid changes of the TiO_2 morphological structures) prior to the deposition of Ag/AgCl, to prepare Ag/AgCl @ broken chiral TiO_2 nanofibers. The synthesis of Ag/AgCl @ broken chiral TiO_2 nanofibers was carried out under the same conditions (the same amount of temples and $AgNO_3$, irradiation time etc.) as Ag/AgCl @ chiral TiO_2 nanofibers to ensure the equal amount of Ag/AgCl depositing on the same amount of chiral TiO_2 nanofibers and broken chiral nanofibers.

Characterization: SEM images were obtained with (JEOL JSM-7041F) at accelerating voltage of 1 kV. TEM was taken using JEOL 2011 operation at 200 kV. XRD patterns were recorded on a Rigaku X-ray diffractometer D/MAX-2200/PC equipped with Cu *Kα* radiation (40 kV, 20 mA). XPS results were obtained with PHI 5000C ESCA with Mg *Kα* source operating at 14 kV and 25 mA. UV-vis diffuse reflectance spectroscopy was performed in triplicate on similar samples to ensure reproducibility using a SHIMADZU UV-2450 with a collection speed of 40 nm min^{-1} and $BaSO_4$ as the reference.

Photocatalytic experiments: The photocatalytic degradation of EE2 was performed

with the powder photocatalyst (0.1 g) suspended in a solution (100 mL) of EE2 (5 mg/L). The light source was a 300W Xe arc lamp (Philips) with a UV cut-off filter (providing visible light $\lambda \geq 400$ nm). The experiments were carried out in a beaker (500 mL) placed under the light, the depth of liquid was 3 cm (see Supplementary Information Fig S1). The concentration of EE2 (after 30 min dark absorption) was detected by High Performance Liquid Chromatography (HPLC, Agilent 1100). Mobile phase of 70% methanol (Merck) and 30% water, flow rate of 0.5 mL/min, injection volume of 10μL, and absorption wavelength of 280 nm.

Reference

S1. P. Wang, B. Huang, Z. Lou, X. Zhang, X. Qin, Y. Dai, Z. Zheng, & X. Wang, Chem. Eur. J., 2010, **16,** 538.

S2. J. Yu, G. Dai, & B. Huang, J. Phys. Chem. C. 2009, **113,** 16394.

S3. W.C. Scott and E. Thimsen, Energy Environ. Sci., 2012, **5,** 5133.

S4. X. Shen, C. Shen, J. Wang, D. Shi, Z. Wang, N. Liu and B. Ding, *J. Am. Chem. Soc*., 2012, **134,** 146.